Contents lists available at ScienceDirect

Physics and Imaging in Radiation Oncology

Original Research Article

Correlations of tumour permeability parameters with apparent diffusion coefficient in nasopharyngeal carcinoma

Alan W.L. Mui [a,b,*], Anne W.M. Lee [b], W.T. Ng [b], Victor H.F. Lee [b], Varut Vardhanabhuti [c], Shei S.Y. Man [a], Daniel T.T. Chua [d], X.Y. Guan [b]

[a] *Department of Radiotherapy, Hong Kong Sanatorium and Hospital, Hong Kong*
[b] *Department of Clinical Oncology, Li Ka Shing Faculty of Medicine, The University of Hong Kong, Hong Kong*
[c] *Department of Diagnostic Radiology, Li Ka Shing Faculty of Medicine, The University of Hong Kong, Hong Kong*
[d] *Department of Medicine, Hong Kong Sanatorium and Hospital, Hong Kong*

A R T I C L E   I N F O

A B S T R A C T

Background and Purpose: Functional imaging has an established role in therapeutic monitoring of cancer treatments. This study evaluated the correlations of tumour permeability parameters derived from dynamic contrast-enhanced magnetic resonance imaging (DCE-MRI) and tumour cellularity derived from apparent diffusion coefficient (ADC) in nasopharyngeal carcinoma (NPC).

Material and Methods: Twenty NPC patients were examined with DCE-MRI and RESOLVE diffusion-weighted MRI (DW-MRI). Tumour permeability parameters were quantitatively measured with Tofts compartment model. Volume transfer constant (K^{trans}), volume of extravascular extracellular space (EES) per unit volume of tissue (V_e), and the flux rate constant between EES and plasma (K_{ep}) from DCE-MRI scan were measured. The time-intensity curve was plotted from the 60 dynamic phases of DCE-MRI. The initial area under the curve for the first 60 s of the contrast agent arrival (iAUC60) was also calculated. They were compared with the ADC value derived from DW-MRI with Pearson correlation analyses.

Results: Among the DCE-MRI permeability parameters, K_{ep} had higher linearity in inverse correlation with ADC value ($r = -0.69$, $p = <0.05$). K^{trans} ($r = -0.60$, $p = <0.05$) and iAUC60 ($r = -0.64$, $p = <0.05$) also had significant inverse correlations with ADC. V_e showed a significant positive correlation with ADC ($r = 0.63$, $p = <0.05$).

Conclusions: Nasopharyngeal tumour vascular permeability parameters derived from DCE-MRI scan were correlated linearly with tumour cellularity measured by free water diffusability with ADC. The clinical implementations of these linear correlations in the quantitative assessments of therapeutic response for NPC patients may be worth to further explore.

1. Introduction

Nasopharyngeal carcinoma (NPC) is a prevalent malignant disease with remarkably high incidence in southern China and Southeast Asia. Intensity-modulated radiotherapy is the standard treatment and has shown excellent tumour control and disease-free survival in the treatment of NPC [1–3]. Concurrent chemotherapy with or without an induction course is also required for locally advanced disease [4].

When a tumour grows larger than 2–3 cubic millimetres in size, oxygen and nutrient supplies by simple diffusion are no longer efficient enough to support the rapid cell proliferation [5]. The tumour oxygen tension triggers the hypoxia-inducible factor 1-alpha (HIF-1α) expression, which in turn induces the release of pro-angiogenic factors. A concentration gradient of pro-angiogenic factors is developed surrounding the hypoxic tumour. When they reaches the nearby blood vessel, they trigger basement membrane degradations and start tip cell migrations. The tip cells migrate towards the hypoxic tumour and form a new blood vessel [6]. This newly formed blood vessel supports the hypoxic tumour with oxygen and nutrients to continue the tumour growth. Hence, aggressive tumours are often highly vascularised [7–9]. On the other hand, tumour plasma perfusion affects the delivery of chemotherapy and thus can affect the treatment outcome for head and

---

* Corresponding author at: Department of Radiotherapy, Hong Kong Sanatorium and Hospital, 2 Village Road, Happy Valley, Hong Kong.
  E-mail address: alan.wl.mui@hksh.com (A.W.L. Mui).

neck cancers. Both perfusion computed tomography (CT) and dynamic contrast-enhanced magnetic resonance imaging (DCE-MRI) are available diagnostic scans for assessing tumour plasma perfusion. Studies have shown that baseline tumour plasma perfusion is predictive in chemotherapy treatment response for patients with head and neck cancers [10,11]. Studies have indicated that tumour permeability is associated with the diffusivity and clinical stage of NPC [12,13].

Reduced diffusivity is associated with tumour cellularity which can be used as an indicator for the evaluation of treatments [14]. Diffusion-weighted magnetic resonance imaging (DW-MRI) is one of the standard diagnostic examinations for detecting the diffusivity within a tumour. Apparent diffusion coefficient (ADC) measures the magnitude of diffusion of water molecules within tissue and is inversely proportional to the tumour cellularity [14]. Studies have shown the values of detecting tumour proliferation potential and predicting early treatment response by analysing the pre-treatment ADC in head and neck cancers [15,16]. Studies have indicated that pre-treatment ADC is a prognostic factor for local relapse-free survival and disease-free survival in NPC [17,18].

Early changes in tumour permeability kinetics have clinical values in monitoring chemotherapy response for NPC [19]. The pre-treatment ADC value was also found to be a clinical indicator of chemotherapy response in patients with NPC [20]. Both tumour permeability kinetics and cellularity can be crucial factors affecting chemotherapy efficacy. To our understanding, the correlations between the tumour permeability kinetics and ADC specific to NPC have not been established. The purpose of this study was to analyse the association between tumour permeability parameters and tumour diffusivity in NPC patients, so as to establish the quantitative relation between angiogenesis and cellularity for the potential therapeutic response monitoring.

2. Materials and Methods

This prospective study was approved by the hospital research ethics committee (REC-2017–06) in compliance with the ethical standards for human research in the Declaration of Helsinki and the Good Clinical Practice (GCP). Informed consent was obtained from the patients.

2.1. Patients

Twenty patients with histopathologically confirmed NPC (Table 1) who underwent helical tomotherapy were examined with DCE-MRI and DW-MRI before starting treatments. There were 16 males (80 %) and 4 females (20 %) with a median age of 47 ± 11.6 years (Range 26–66 years). All of them were classified based on the 2017 American Joint Committee of Cancer (AJCC) TNM classification of malignant tumours (8th Edition) [21] as stage II or above who were eligible for chemoradiation treatments.

2.2. MR imaging

The MR scans were originally used for radiation therapy planning. For that reason, all patients were immobilised in thermoplastic casts and scanned with a 1.5 T MAGNETOM Aera MR Simulator (Siemens Healthcare, Erlangen, Germany) dedicated to radiotherapy planning with gradient performance at maximum amplitude 45mT/m and maximum slew rate of 200mT/m/ms. It is equipped with a 70 cm wide bore and an external laser system for precise patient positioning. The scans were done on a flat couch embedded with a posterior 32-channel spine coil array and a pair of 4-channel large flex receiver coils with interfaces which were wrapped around the head region with a pair of bilateral coil holders (Orfit Industry, Wijnegem, Belgium). In order to avoid any retained contrast agent from DCE-MRI which might affect the accuracy of DW-MRI measurement, the DW-MRI was scanned before the DCE-MRI.

2.2.1. DW-MRI

The primary nasopharyngeal lesion of the patient was localised based on the non-contrast morphological images and previous diagnostic radiological reports. The axial DW-MRI images were acquired in an interleaved fashion using a 2D diffusion-weighted multi-shot readout-segment echo-planar imaging (RS-*EPI*) RESOLVE sequence with GRAPPA acceleration technique. The imaging parameters of DW-MRI were set as FOV 220×220 mm; matrix size of 112×112; slice thickness of 3.5 mm with 10 % gap; voxel size of $2 \times 2 \times 3.5$ mm; slice number of 20; phase encoding in anteroposterior direction; TR/TE1/TE2 of 3890/51/78 ms (TE1 as the segment echo and TE2 as the navigator echo for phase correction between shots). Diffusion sensitivities (b-values) at high (800 *sec*/mm^2) with average factor of 4 and low (50 *sec*/mm^2) with average factor of 2 were selected. The DW-MRI scans were acquired in 6 min 27 s. The scan volume was set as contiguous axial sections through the primary nasopharyngeal lesion. The rate of diffusion is evaluated by these images with different b-values and quantitatively represented by ADC map.

2.2.2. DCE-MRI

In order to measure the contrast enhancement pattern in the tumour, two axial pre-contrast 3D T1-weighted spoiled gradient-echo (GRE) VIBE sequences using flip angles of 2 and 15 degrees were performed respectively for baseline mapping. These flip angles were chosen as this combination achieved the smallest overestimation for K^{trans} in primary tumours of head and neck cancers [22]. The T1 mapping was scanned with FOV of 260×260 mm; matrix size of 192×154; slice thickness of 3.5 mm; voxel size of $1.4 \times 1.4 \times 3.5$ mm; slice number of 30; TR/TE of 3.8/1.34 ms. Once T1 mapping was performed, the acquisition of DCE-MRI images with the same coverage was started for 3 dynamic phases before the administration of gadobutrol contrast agent. A dose of 0.1 mmol/kg of gadobutrol (Gadovist, Bayer Vital GmbH, Leverkusen, Germany) contrast agent was injected using a power injector at a constant flow rate of 2.5 mL/*sec* followed by a 20 mL normal saline flushed at the same flow rate. The DCE-MRI was performed using an axial 3D T1-weighted TWIST VIBE sequence with the following parameters: FOV 260×260 mm; matrix size of 192×154; slice thickness of 3.5 mm; voxel size of $1.4 \times 1.4 \times 3.5$ mm; slice number of 30; TR/TE of 6.28/2.38 ms; and flip angle of 9 degrees. A total of 60 dynamic phases with temporal resolution of 4.7 s were acquired. The total acquisition time of approximately 4 min 42 s.

The imaging protocols of the DW-MRI and DCE-MRI scans are summarized in Table 2.

Table 1
Patient and tumour characteristics.

Patient Characteristics		No. of Patient	%
Age			
	Range 26–66		
	Median 47		
Sex			
	Male	16	80
	Female	4	20
Pathologic T classification			
	T1	7	35
	T2	3	15
	T3	6	30
	T4	4	20
Stage			
	II	4	20
	III	10	50
	IV	6	30

Table 2
Imaging protocols of DW-MRI and DCE-MRI.

Parameter	DW-MRI	DCE-MRI
Slice orientation	Transversal	Transversal
TR (ms)	3890	6.28
TE (ms)	51/78	2.38
b values (s/mm^2)	50(2), 800(4)	
Voxel size (mm^3)	$2 \times 2 \times 3.5$	$1.4 \times 1.4 \times 3.5$
Field of view (mm^2)	220×220	260×260
Matrix	112×112	192×154
Slice thickness (mm)	3.5	3.5
Slice gap (mm)	0.35	
No. of slices	20	30
Fat suppression	SPAIR	CHESS
Readout segments	7 shots	
Readout partial Fourier acquisition	5/8	
GRAPPA acceleration factor	2	
Flip angle	180°	9°
Acquisition time (min:s)	6:27	4:42

2.3. Post-processing

All the DCE-MRI and DW-MRI image series were post-processed by the image reading application syngo.via (Siemens Healthcare, Erlangen, Germany) developed by MR Simulator vendor. Tumour permeability parameters were quantitatively measured with Tofts compartment model [23,24]. In the Tofts model, each voxel of tissue is differentiated into tissue parenchymal cells, blood vessels and tissue extracellular extravascular space (EES). The influx rate from blood vessels into EES can be measured as volume transfer constant (K^{trans}) and the reflux rate from EES back into plasma can be measured as flux rate constant (K_{ep}) with gadolinium contrast administration [24]. The volume of EES per unit volume of tissue (V_e) can also be depicted with the perfusion model. The arterial input function (AIF) was modelled to the gadobutrol contrast agent according to the Tofts model by population-based technique [25] with the AIF curve best fitted to either fast [26], intermediate [27] or slow [28] population-averaged AIF. The K^{trans}, V_e and K_{ep} from the DCE-MRI scan were measured by positioning a volume of interest

(VOI) at the primary nasopharyngeal tumour localised by reviewing patient's recent diagnostic MR and/or positron emission tomography (PET) scans at where distinct contrast enhancement and/or elevated standardised uptake value (SUV) were observed. The MR signal intensity time course in DCE-MRI was represented by the time-intensity curve (TIC). It was plotted from the 60 dynamic phases of DCE-MRI. The initial area under curve for the first 60 s of the contrast agent arrival (iAUC60) was also calculated. All K^{trans}, V_e, K_{ep} and iAUC60 were compared with the ADC value from DW-MRI with Pearson correlation analyses. The K^{trans} was compared with disease stages by Kruskal-Wallis test.

3. Results

Examples of the DCE-MRI and DW-MRI images are shown in Fig. 1.
Patients with higher TNM-staged diseases tended to have slightly higher median K^{trans} values. The median K^{trans} for stage II, III and IV diseases were 0.10 min^{-1} (range 0.06–0.23 min^{-1}), 0.13 min^{-1} (range
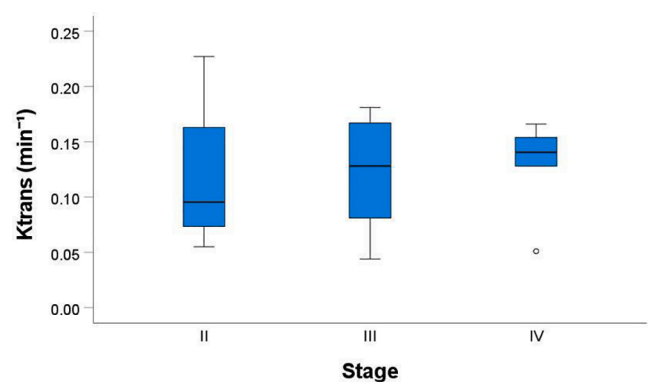

Fig. 2. The Box-and-whisker plot of K^{trans} values from DCE-MRI among patients with different disease stages. The medians and ranges are shown. The bottom and top edges of boxes represent the 1st and the 3rd quartiles of values respectively.
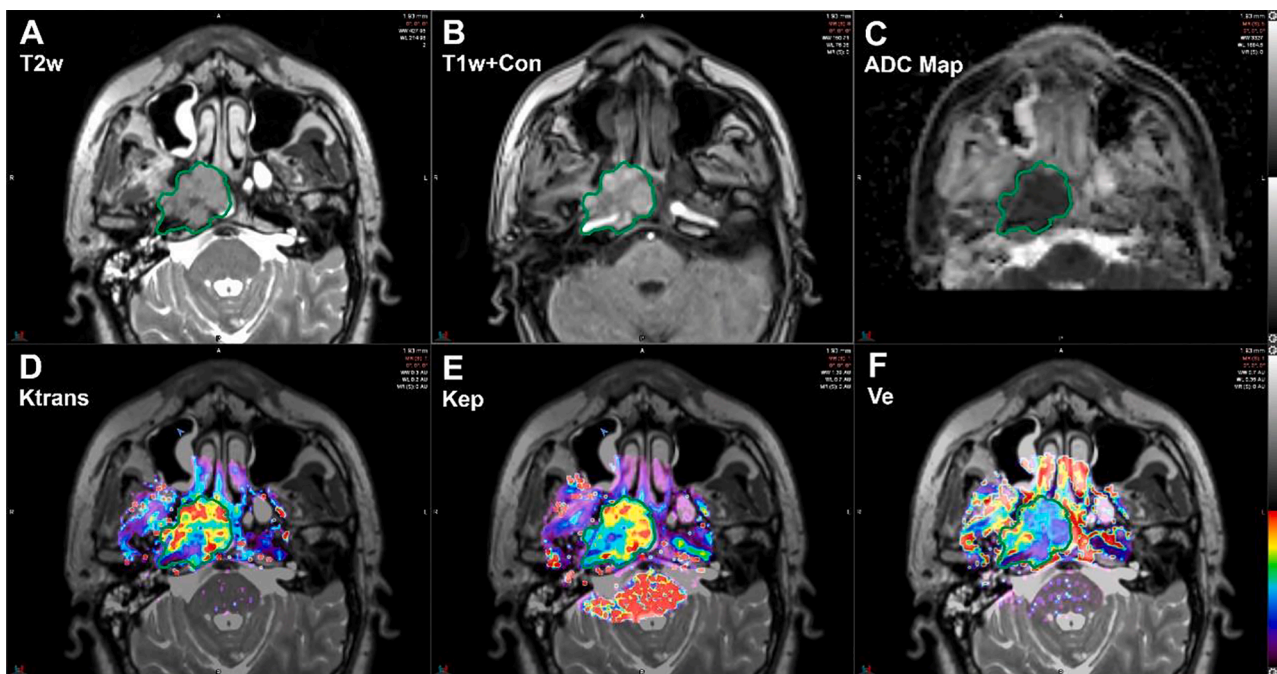

Fig. 1. DCE-MRI and DW-MRI scans of an NPC patient with a T3 staged tumour. Morphological T2-weighted image (A), contrast-enhanced T1-weighted image (B) and ADC map (C) are shown. The corresponding permeability parametric maps from DCE-MRI including K^{trans} (D), K_{ep} (E) and V_e (F) are shown on the lower row. The gross tumour volume (GTV) is delineated in green.

0.04–0.18 min^{-1}) and 0.14 min^{-1} (range 0.05–0.17 min^{-1}) respectively (Fig. 2). A mild increase of K^{trans} was observed versus increase in disease stage although statistical significances could not be obtained (p = 0.871).

The correlations of permeability parameters from DCE-MRI with ADC from DW-MRI are shown in regression plots in Fig. 3. All the permeability parameters acquired by DCE-MRI in NPC tumours showed significant linear correlations with ADC value. The K^{trans} (r = −0.60, p = <0.05), K$_{ep}$ (r = −0.69, p = <0.05) and iAUC60 (r = −0.64, p = <0.05) showed significant inverse correlations with ADC value whereas the V$_e$ showed a significant positive correlation with ADC (r = 0.63, p = <0.05).

4. Discussions

This study has shown that tumour cellularity as reflected by ADC was linearly associated with the vascular permeability in nasopharyngeal tumours. In particular, we have identified the reflux rate which was the parameter with the strongest inverse linear correlation with the ADC. This linear correlation between tumour cellularity and vascular permeability in nasopharyngeal tumour might be worth to further investigate for its implementations in therapeutic response monitoring of NPC patients.

Our findings in tumour cellularity and permeability correlation were consistent with known nasopharyngeal tumour biology [9,29,30]. Advanced tumour proliferates vigorously, which needs steady supplies of oxygen and nutrients to support the active cell replications. This

process is facilitated by tumour angiogenesis. The tumour grows by absorbing oxygen and nutrients for its rapid cell proliferation. In this study, we found that NPC patients with reduced ADC were associated with higher tumour permeability. The K^{trans} and K$_{ep}$ were inversely correlated with the ADC value in nasopharyngeal tumours, which agreed with the phenomenon of active tumour angiogenesis for advanced tumours with high cellularity [31–33]. In particular, the K$_{ep}$ exhibited stronger inverse correlation with ADC. This may be explained by the fact that increased vascular permeability promotes additional extravasation of plasma in combination with the effect that the increased tumour cellularity narrows the EES. Both factors contribute to an increase in EES pressure which potentiates a flux tension from EES to plasma. Therefore, the K$_{ep}$, reflecting the flux rate constant between the EES and plasma, had higher linearity in inverse correlation.

Advanced tumours are usually densely packed with highly proliferative cells. The presence of numerous membranous and macromolecular structures impedes the free water diffusability within the tumour. The increased cellularity occupies the space within the tumour so that the volume of EES per unit volume of tissue decreases. The V$_e$ in the Tofts model measures the EES per unit volume of tissue and is mathematically calculated by V$_e$ = K^{trans}/K$_{ep}$. The V$_e$ represents the ratio of K^{trans} to K$_{ep}$. We have found a significant positive correlation of the V$_e$ with the ADC. This positive correlation between V$_e$ and ADC in nasopharyngeal tumour agrees with permeability and diffusability study findings from other tumours including prostate and brain cancers [34–36]. However, it is not the same with some breast cancer studies in which negative correlations between V$_e$ and ADC were reported [37,38]. One of their
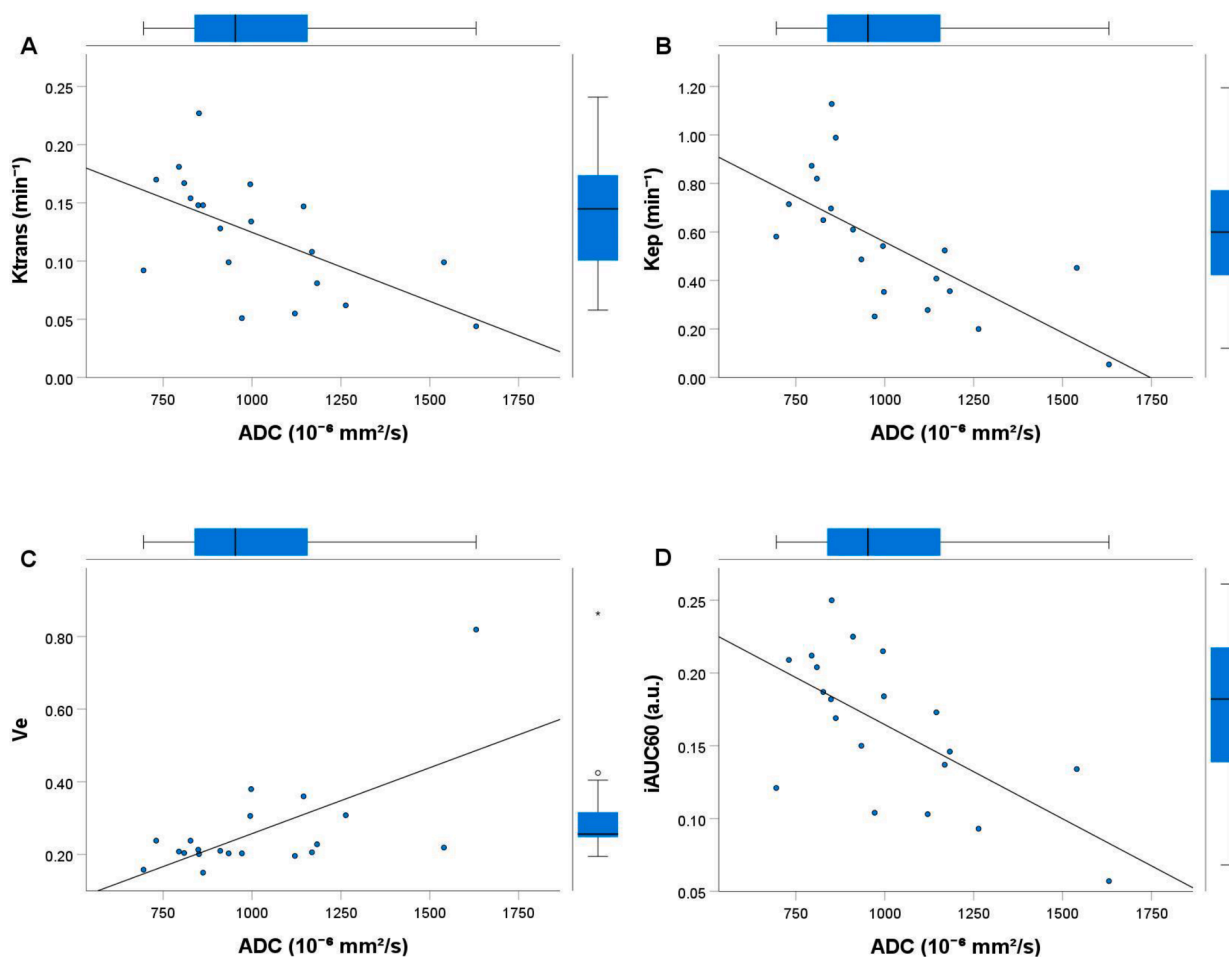

Fig. 3. Regression plots of permeability parameters from DCE-MRI for K^{trans} (A), K$_{ep}$ (B), V$_e$ (C) and iAUC60 (D) against ADC value from DW-MRI. The Box-and-whisker plots of the corresponding vascular permeability parameters and ADC are also shown to demonstrate their distributions. The bottom/left and top/right edges of boxes represent the 1st and the 3rd quartiles of values respectively.

postulations for this contrary correlation in breast cancer is that non-invasive ductal carcinoma and malignant phyllodes tumours with bleeding consist of necrotic centre, haemorrhage and calcification with lower cellular density than normal breast tissues. The increased ADC value in breast tumours attributes to these lowered cellular density characteristics [39].

The iAUC60 value manifests the macroscopic permeability characteristics of a tumour by summarising the contrast agent flush in and early wash out in the initial period of 60 s on the TIC. Studies have shown that malignant tumours with high cellularity tend to have rapid early enhancement with a short time to intensity peak followed by a clear washout on their TIC [40–42]. In this study, we have found that these TIC characteristics were also valid in the nasopharyngeal tumour. Patients with lower ADC values were found to have higher iAUC60 in our cohort of patients. Nasopharyngeal tumours with higher cellularity and lower diffusability are leakier in vasculature than others [43]. It suggests that advanced nasopharyngeal tumour with high cellularity tends to have well-developed permeable vasculature, which is distinctly efficient in supporting proliferation and growth.

We have found that ADC is linearly associated with the vascular permeability in nasopharyngeal tumours in our study cohort. Diffusion restriction as measured by ADC has been used as an indicator of tumour cellularity and could explain the association with perfusion as demonstrated here, although we acknowledge that DW-MRI at low b-values is sensitive to perfusion effects, and that a low b-value of 50 s/mm^2 as chosen in our study, may not fully suppress the influence of perfusion on the measured ADC values. Despite this, our findings are in line with several prior studies supporting the hypothesis that proliferative tumours with higher cellularity are likely to have higher vascular permeability. Ni, Liu [13] reported in their study for NPC with DCE-MRI and DW-MRI scans using a 3T MR scanner, that a negative correlation was found with K^{trans} and ADC in their cohort. Our results support their findings regarding K^{trans} and ADC correlation. They also revealed that the clinical stage of NPC was positively correlated with K^{trans}. We also observed a similar trend in our cohort though statistical significance was not achieved. Kooreman, et al. [44] reported an inverse correlation between diffusion coefficient (D) and perfusion fraction (f) in prostate cancer with intravoxel incoherent motion (IVIM) MRI using MR-Linac. Pre-treatment prostatic tumours were found to have lower D but higher f than non-cancerous prostates. Chu, et al. [36] also reported in their study for brain tumours with DCE-MRI and DW-MRI scans, that a similar inverse correlation between tumour permeability and diffusability was found. They identified that brain tumours were characterised by lower ADC values but higher volume transfer constant K^{trans}. In our cohort of nasopharyngeal tumours, albeit both K^{trans} and K_{ep} were found to have significant correlations with ADC, we have found that the flux rate constant K_{ep} has a higher linearity in inverse correlation with ADC values than the K^{trans} among the permeability parameters. Svolos, et al. [35] also investigated the permeability and diffusability of brain tumours based on multi-parametric MRI scans including DW-MRI, diffusion tensor imaging (DTI) and dynamic-susceptibility contrast imaging (DSCI). They noticed that vascularity and cellularity were factors closely related in brain tumours but they were correlated in a non-linear manner. On the contrary, we observed that this vascularity and cellularity correlation, reflected by permeability and diffusability respectively, was relatively linear in our cohort of nasopharyngeal tumours.

The changes in these correlations between tumour permeability and diffusability after the commencement of chemotherapy treatments can reflect the status changes in angiogenesis and cellularity. Since we have found significant linear correlations between parameters of tumour permeability and diffusability, the clinical implementations of these linear correlations in the quantitative assessments of therapeutic response for NPC patients may be worth to further explore. DCE-MRI is more informative than DW-MRI in which the influx rate from blood vessels into EES and the reflux rate from EES back into plasma can be differentiated for further studies in their individual value for therapeutic

response monitoring of NPC. These permeability characteristics can be differentially visualised in parametric maps. As concurrent chemo-radiation is the standard treatment for locally advanced NPC patients, these parametric maps might be useful in monitoring angiogenic changes during chemo-radiation treatments [45]. Since we acquired the scans with an MR Simulator in which the patients were scanned in the same positions as their radiation treatment positions, the parametric maps had the same frame of reference as their radiation treatment plans. The parametric maps might be possible to use for radiation treatment customisations and adaptations with tumour biological changes [46].

Our study on the correlation of permeability parameters and ADC in NPC has limitations. The sample size is relatively small, and further recruitment of NPC patients in this study is needed to arrive at a more robust observation of permeability and diffusivity. Stratification of patients by different *T*-stages will also be possible with a larger cohort to see if there is any difference in correlations with different tumour sizes. In order to maintain a high temporal resolution for TIC, the DCE-MRI was scanned with limited anatomical coverage to the primary nasopharyngeal tumour only. Cervical lymphatics were not included in the DCE-MRI scans in our study. Further studies including the investigations in permeability and diffusion correlations at cervical lymph nodes are worth considering for a more comprehensive understanding of NPC.

In conclusion, nasopharyngeal tumour vascular permeability parameters derived from DCE-MRI scan were correlated linearly with cellularity measured by free water diffusability with ADC. The clinical implementations of these linear correlations in the quantitative assessments of therapeutic response for NPC patients may be worth to further explore.

Declaration of Competing Interest

The authors declare that they have no known competing financial interests or personal relationships that could have appeared to influence the work reported in this paper.

References

[1] Sun X, Su S, Chen C, Han F, Zhao C, Xiao W, et al. Long-term outcomes of intensity-modulated radiotherapy for 868 patients with nasopharyngeal carcinoma: an analysis of survival and treatment toxicities. Radiother Oncol 2014;110:398–403. https://doi.org/10.1016/j.radonc.2013.10.020.

[2] Lertbutsayanukul C, Prayongrat A, Kannarunimit D, Chakkabat C, Netsawang B, Kitpanit S. A randomized phase III study between sequential versus simultaneous integrated boost intensity-modulated radiation therapy in nasopharyngeal carcinoma. Strahlenther Onkol 2018;194:375–85. https://doi.org/10.1007/s00066-017-1251-5.

[3] Lee AWM, Sze WM, Au JSK, Leung SF, Leung TW, Chua DTT, et al. Treatment results for nasopharyngeal carcinoma in the modern era: The Hong Kong experience. Int J Radiat Oncol Biol Phys 2005;61:1107–16. https://doi.org/10.1016/j.ijrobp.2004.07.702.

[4] Blanchard PMD, Lee AP, Marguet SM, Leclercq JM, Ng WTMD, Ma JP, et al. Chemotherapy and radiotherapy in nasopharyngeal carcinoma: an update of the MAC-NPC meta-analysis. Lancet Oncol 2015;16:645–55. https://doi.org/10.1016/S1470-2045(15)70126-9.

[5] Folkman J. Anti-angiogenesis: new concept for therapy of solid tumors. Ann Surg 1972;175:409–16. http://www.ncbi.nlm.nih.gov/pmc/articles/PMC1355186/.

[6] McMahon G. VEGF receptor signaling in tumor angiogenesis. Oncologist 2000;5: 3–10. https://doi.org/10.1634/theoncologist.5-suppl_1-3.

[7] Arnold F. Tumour angiogenesis. Ann R Coll Surg Engl 1985;67:295–8.

[8] Lentsch EJ, Goudy S, Sosnowski J, Major S, Bumpous JM. Microvessel density in head and neck squamous cell carcinoma primary tumors and its correlation with clinical staging parameters. Laryngoscope 2006;116:397–400. https://doi.org/10.1097/01.MLG.0000195286.29613.E1.

[9] Xueguan L, Xiaoshen W, Yongsheng Z, Chaosu H, Chunying S, Yan F. Hypoxia inducible factor-1α and vascular endothelial growth factor expression are associated with a poor prognosis in patients with nasopharyngeal carcinoma receiving radiotherapy with carbogen and nicotinamide. Clin Oncol 2008;20: 606–12. https://doi.org/10.1016/j.clon.2008.07.001.

[10] Singh K, Sunku R, Rathi AK, Pradhan GS. Predicting outcome of advanced head-and-neck cancer by measuring tumor blood perfusion in patients receiving neoadjuvant chemotherapy. J Cancer Res Ther 2020;16:S34–8. https://doi.org/10.4103/jcrt.JCRT_195_18.

[11] Bernstein JM, Kershaw LE, Withey SB, Lowe NM, Homer JJ, Slevin NJ, et al. Tumor plasma flow determined by dynamic contrast-enhanced MRI predicts response to

induction chemotherapy in head and neck cancer. Oral Oncol 2015;51:508–13. https://doi.org/10.1016/j.oraloncology.2015.01.013.

[12] Sriyook A, Lertbutsayanukul C, Jittapiromsak N. Value of dynamic contrast-enhanced magnetic resonance imaging for determining the plasma Epstein-Barr virus status and staging of nasopharyngeal carcinoma. Clin Imaging 2021;72:1–7. https://doi.org/10.1016/j.clinimag.2020.10.047.

[13] Ni L, Liu Y. Contrast-enhanced dynamic and diffusion-weighted magnetic resonance imaging at 3.0 T to assess early-stage nasopharyngeal carcinoma. Oncol Lett 2018;15:5294–300. https://doi.org/10.3892/ol.2018.7948.

[14] Descoteaux M, Poupon C. Diffusion-weighted MRI. In: Belkić D, Belkić K, editors. Comprehensive biomedical physics: magnetic resonance imaging and spectroscopy. Stockholm: Elsevier B.V; 2014. p. 81–97. https://doi.org/10.1016/b978-0-444-53632-7.00306-3.

[15] Kim S, Loevner L, Quon H, Sherman E, Weinstein G, Kilger A, et al. Diffusion-weighted magnetic resonance imaging for predicting and detecting early response to chemoradiation therapy of squamous cell carcinomas of the head and neck. Clin Cancer Res 2009;15:986–94. https://doi.org/10.1158/1078-0432.CCR-08-1287.

[16] Surov A, Meyer HJ, Winter K, Richter C, Hoehn A-K. Histogram analysis parameters of apparent diffusion coefficient reflect tumor cellularity and proliferation activity in head and neck squamous cell carcinoma. Oncotarget 2018; 9:23599-607. 10.18632/oncotarget.25284.

[17] Zhang Y, Liu X, Zhang Y, Li W-F, Chen L, Mao Y-P, et al. Prognostic value of the primary lesion apparent diffusion coefficient (ADC) in nasopharyngeal carcinoma: a retrospective study of 541 cases. Sci Rep 2015;5:12242. https://doi.org/10.1038/srep12242.

[18] Yan D-F, Zhang W-B, Ke S-B, Zhao F, Yan S-X, Wang Q-D, et al. The prognostic value of pretreatment tumor apparent diffusion coefficient values in nasopharyngeal carcinoma. BMC Cancer 2017;17:678. https://doi.org/10.1186/s12885-017-3658-x.

[19] Zheng D, Yue Q, Ren W, Liu M, Zhang X, Lin H, et al. Early responses assessment of neoadjuvant chemotherapy in nasopharyngeal carcinoma by serial dynamic contrast-enhanced MR imaging. Magn Reson Imaging 2017;35:125–31. https://doi.org/10.1016/j.mri.2016.08.011.

[20] Zhang GY, Wang YJ, Liu JP, Zhou XH, Xu ZF, Chen XP, et al. Pretreatment diffusion-weighted MRI can predict the response to neoadjuvant chemotherapy in patients with nasopharyngeal carcinoma. Biomed Res Int 2015;2015:307943. https://doi.org/10.1155/2015/307943.

[21] Brierley J, Gospodarowicz MK, Wittekind C. TNM classification of malignant tumours. Eighth edition. ed. Chichester, West Sussex, UK, Hoboken, NJ: John Wiley & Sons, Inc.; 2017.

[22] Yuan J, Chow SKK, Yeung DKW, Ahuja AT, King AD. Quantitative evaluation of dual-flip-angle T1 mapping on DCE-MRI kinetic parameter estimation in head and neck. Quant Imaging Med Surg 2012;2:245–53. https://doi.org/10.3978/j.issn.2223-4292.2012.11.04.

[23] Tofts PS, Brix G, Buckley DL, Evelhoch JL, Henderson E, Knopp MV, et al. Estimating kinetic parameters from dynamic contrast-enhanced T(1)-weighted MRI of a diffusable tracer: standardized quantities and symbols. J Magn Reson Imaging 1999;10:223–32. https://doi.org/10.1002/(SICI)1522-2586(199909)10:3<223::AID-JMRI2>3.0.CO;2-S.

[24] Tofts PS. Modeling tracer kinetics in dynamic Gd-DTPA MR imaging. J Magn Reson Imaging 1997;7:91–101. https://doi.org/10.1002/jmri.1880070113.

[25] Rata M, Collins DJ, Darcy J, Messiou C, Tunariu N, Desouza N, et al. Assessment of repeatability and treatment response in early phase clinical trials using DCE-MRI: comparison of parametric analysis using MR- and CT-derived arterial input functions. Eur Radiol 2016;26:1991–8. https://doi.org/10.1007/s00330-015-4012-9.

[26] Orton MR, d'Arcy JA, Walker-Samuel S, Hawkes DJ, Atkinson D, Collins DJ, et al. Computationally efficient vascular input function models for quantitative kinetic modelling using DCE-MRI. Phys Med Biol 2008;53:1225–39. https://doi.org/10.1088/0031-9155/53/5/005.

[27] Parker GJM, Roberts C, Macdonald A, Buonaccorsi GA, Cheung S, Buckley DL, et al. Experimentally-derived functional form for a population-averaged high-temporal-resolution arterial input function for dynamic contrast-enhanced MRI. Magn Reson Med 2006;56:993–1000. https://doi.org/10.1002/mrm.21066.

[28] Weinmann HJ, Laniado M, MÜTzel W. Pharmacokinetics of GdDTPA/dimeglumine after intravenous injection into healthy volunteers. Physiol Chem Phys Med NMR 1984;16:167–72.

[29] Hong B, Lui VWY, Hashiguchi M, Hui EP, Chan A-T-C. Targeting tumor hypoxia in nasopharyngeal carcinoma. Head Neck 2013;35:133–45. https://doi.org/10.1002/hed.21877.

[30] Hui EP, Chan ATC, Pezzella F, Turley H, To K-F, Poon TCW, et al. Coexpression of hypoxia-inducible factors 1alpha and 2alpha, carbonic anhydrase IX, and vascular endothelial growth factor in nasopharyngeal carcinoma and relationship to survival. Clin Cancer Res 2002;8:2595–604.

[31] Walsh JJ, Parent M, Akif A, Adam LC, Maritim S, Mishra SK, et al. Imaging hallmarks of the tumor microenvironment in glioblastoma progression. Front Oncol 2021;11:692650. 10.3389/fonc.2021.692650.

[32] Meyer H-J, Hamerla G, Leifels L, Höhn AK, Surov A. Histogram analysis parameters derived from DCE-MRI in head and neck squamous cell cancer – Associations with microvessel density. Eur J Radiol 2019;120:108669. https://doi.org/10.1016/j.ejrad.2019.108669.

[33] Chu JP, Mak HK, Yau KK, Zhang L, Tsang J, Chan Q, et al. Pilot study on evaluation of any correlation between MR perfusion (Ktrans) and diffusion (apparent diffusion coefficient) parameters in brain tumors at 3 Tesla. Cancer Imaging 2012;12:1–6. https://doi.org/10.1102/1470-7330.2012.0001.

[34] Pang Y, Turkbey B, Bernardo M, Kruecker J, Kadoury S, Merino MJ, et al. Intravoxel incoherent motion MR imaging for prostate cancer: An evaluation of perfusion fraction and diffusion coefficient derived from different b-value combinations. Magn Reson Med 2013;69:553–62. https://doi.org/10.1002/mrm.24277.

[35] Svolos P, Tsolaki E, Kapsalaki E, Theodorou K, Fountas K, Fezoulidis I, et al. Investigating brain tumor differentiation with diffusion and perfusion metrics at 3T MRI using pattern recognition techniques. Magn Reson Imaging 2013;31:1567–77. https://doi.org/10.1016/j.mri.2013.06.010.

[36] Chu J-P, Mak HK-F, Yau KK-W, Zhang L, Tsang J, Chan Q, et al. Pilot study on evaluation of any correlation between MR perfusion (K trans) and diffusion (apparent diffusion coefficient) parameters in brain tumors at 3 Tesla. Cancer Imaging 2012;12:1-6. 10.1102/1470-7330.2012.0001.

[37] Li T, Yu T, Li L, Lu L, Zhuo Y, Lian J, et al. Use of diffusion kurtosis imaging and quantitative dynamic contrast-enhanced MRI for the differentiation of breast tumors. J Magn Reson Imaging 2018;48:1358–66. https://doi.org/10.1002/jmri.26059.

[38] Yankeelov TE, Lepage M, Chakravarthy A, Broome EE, Niermann KJ, Kelley MC, et al. Integration of quantitative DCE-MRI and ADC mapping to monitor treatment response in human breast cancer: initial results. Magn Reson Imaging 2007;25:1–13. https://doi.org/10.1016/j.mri.2006.09.006.

[39] Abdel Razek AAKMD, Gaballa GMD, Denewer AMD, Tawakol IMD. Diffusion weighted MR imaging of the breast. Acad Radiol 2010;17:382–6. https://doi.org/10.1016/j.acra.2009.10.014.

[40] Furukawa M, Parvathaneni U, Maravilla K, Richards TL, Anzai Y. Dynamic contrast-enhanced MR perfusion imaging of head and neck tumors at 3 Tesla. Head Neck 2013;35:923–9. https://doi.org/10.1002/hed.23051.

[41] Pickles MD, Lowry M, Manton DJ, Gibbs P, Turnbull LW. Role of dynamic contrast enhanced MRI in monitoring early response of locally advanced breast cancer to neoadjuvant chemotherapy. Breast Cancer Res Treat 2005;91:1–10. https://doi.org/10.1007/s10549-004-5819-2.

[42] Knopp MV, Tengg-Kobligk HV, Choyke PL. Functional magnetic resonance imaging in oncology for diagnosis and therapy monitoring. Mol Cancer Ther 2003;2:419–26.

[43] Xiao B, Wang P, Zhao Y, Liu Y, Ye Z. Combination of diffusion-weighted imaging and arterial spin labeling at 3.0 T for the clinical staging of nasopharyngeal carcinoma. Clin Imaging 2020;66:127–32. https://doi.org/10.1016/j.clinimag.2020.05.007.

[44] Kooreman ES, van Houdt PJ, Keesman R, van Pelt VWJ, Nowee ME, Pos F, et al. Daily intravoxel incoherent motion (IVIM) in prostate cancer patients during MR-guided radiotherapy-A multicenter study. Front Oncol 2021;11:705964. https://doi.org/10.3389/fonc.2021.705964.

[45] Pham TT, Liney G, Wong K, Henderson C, Rai R, Graham PL, et al. Multi-parametric magnetic resonance imaging assessment of whole tumour heterogeneity for chemoradiotherapy response prediction in rectal cancer. Phys Imaging Radiat Oncol 2021;18:26–33. https://doi.org/10.1016/j.phro.2021.03.003.

[46] Brighi C, Verburg N, Koh ES, Walker A, Chen C, Pillay S, et al. Repeatability of radiotherapy dose-painting prescriptions derived from a multiparametric magnetic resonance imaging model of glioblastoma infiltration. Phys Imaging Radiat Oncol 2022;23:8–15. https://doi.org/10.1016/j.phro.2022.06.004.